TU Delft

Delft University of Technology

Document Version
Final published version

Licence
CC BY

Citation (APA)
Hupkes, J., Bruna, P. O., Rongier, G., Bertotti, G., Caudroit, J., & Moscariello, A. (2026). Subjective and objective bias in borehole image fracture interpretations. *Geoenergy Science and Engineering*, *268*, Article 214793. https://doi.org/10.1016/j.geoen.2026.214793

Important note
To cite this publication, please use the final published version (if applicable).
Please check the document version above.

Copyright
In case the licence states “Dutch Copyright Act (Article 25fa)”, this publication was made available Green Open Access via the TU Delft Institutional Repository pursuant to Dutch Copyright Act (Article 25fa, the Taverne amendment). This provision does not affect copyright ownership.
Unless copyright is transferred by contract or statute, it remains with the copyright holder.

Sharing and reuse
Other than for strictly personal use, it is not permitted to download, forward or distribute the text or part of it, without the consent of the author(s) and/or copyright holder(s), unless the work is under an open content license such as Creative Commons.

Takedown policy
Please contact us and provide details if you believe this document breaches copyrights.
We will remove access to the work immediately and investigate your claim.

This work is downloaded from Delft University of Technology.

268 (2027) 214793

Contents lists available at ScienceDirect

Geoenergy Science and Engineering

journal homepage: www.sciencedirect.com/journal/geoenergy-science-and-engineering

Subjective and objective bias in borehole image fracture interpretations

Jasper Hupkes[a,*], Pierre-Olivier Bruna[a], Guillaume Rongier[a], Giovanni Bertotti[a], Jerôme Caudroit[b], Andrea Moscariello[c]

[a] Department of Geoscience and Engineering, Delft University of Technology, Stevinweg 1, Delft, 2628 CN, the Netherlands
[b] Services Industriel de Genève, Geneva, Switzerland
[c] Department of Earth Sciences, University of Geneva, Geneva, Switzerland

HIGHLIGHTS

- Five interpretations of one borehole image from a fractured geothermal reservoir in the Geneva Basin are compared.
- Interpretations of the borehole images are prone to interpreter bias.
- Deriving reliable fracture parameters such as frequency and orientation from the borehole image logs is not trivial.
- Lithology appears to exert the largest control on variability of fracture frequency.
- The dip angle of bedding affects the reliability of orientation interpretations.
- Awareness of objective geological bias can help in providing guidelines to improve borehole image interpretations.

ARTICLE INFO

Keywords:
Borehole images
Geneva Basin
Carbonate geothermal reservoir
Natural fractures
Multi-interpretations
Uncertainty
Bias

ABSTRACT

Mitigating bias in geological interpretations in the domain of structural geology and more specifically in seismic images and outcrop data is a well-known challenge. So far, the same issue in borehole image interpretation has rarely been addressed, even though these data are crucial for our knowledge of the subsurface. The Lower Cretaceous carbonate rocks of the Geneva Basin, Switzerland is a naturally fractured geothermal reservoir which has been penetrated by the GEo-01 well. Borehole images of this well were interpreted independently by five interpreters offering a unique database to compare and contrast. In this study we analyzed the impact of lithology and borehole image quality/complexity on the frequency and orientation of fracture picks acquired by the five interpreters. For the fracture frequency, we demonstrate that in GEo-01, the lithology sets the baseline for the level of agreement between the different interpreters, while image quality/complexity plays only a moderate role. On the other hand, the variability between interpretations of the fracture orientation appears mainly to be affected by the dip of strata, where a trend is observed between intervals with low bedding dip angles and more consistent feature orientation picking. As a recommendation for future exploration in the Geneva Basin and beyond, we suggest guidelines based on the geological context of the well in order to increase the value of borehole image interpretations.

1. Introduction

Natural fractures are common features in unconventional geothermal reservoirs, and they can form complex networks that control the fluid flow. Several attributes of the fracture network, expressed as statistical distributions, are essential to characterize these networks at depth: density, orientation, size (height and length) and aperture (Lorenz and Cooper, 2020). However, these attributes are challenging to obtain as a large portion of the fractures are invisible in the subsurface with conventional seismic methods (Boersma et al., 2021; Smith et al., 2024). In this context, the only direct accessibility we have to obtain that information from the underground is provided by boreholes (Wellmann and Caumon, 2018).

Borehole data are generally obtained from cores and borehole images (BHI). Cores are the only direct way of obtaining a sampling of the rocks at depth. They hold key information on single fractures, such as the aperture and fracture type, and sometimes they provide cross-cutting relationships between multiple fractures (Lorenz and Cooper, 2020). However, cores are expensive and challenging to obtain (i.e., due

* Corresponding author.
Email address: j.hupkes@tudelft.nl (J. Hupkes).

https://doi.org/10.1016/j.geoen.2026.214793
Received 22 January 2026; Received in revised form 31 August 2026; Accepted 1 September 2026
Available online 2 September 2026
2949-8910/© 2026 The Author(s). Published by Elsevier B.V. This is an open access article under the CC BY license (http://creativecommons.org/licenses/by/4.0/).

to jamming issues and poor recovery of fractured intervals), so most boreholes will not have a cored interval. In contrast, borehole images are a cost-effective alternative to coring and are therefore more widely available. Borehole image is a generic term defining optical and/or geophysical measures conducted on the walls of a well. Optical borehole images (OBI) are obtained by a camera equipped with a light source measuring the colour spectrum along the borehole, resulting in images with resolution in the order of 0.5–2 mm (Williams and Johnson, 2004). These images are often combined with geophysical borehole images that are based on measures of the electric resistivity or the acoustic impedance (ABI), which typically have a lower resolution (Wood, 2024, 0.5-2 cm). Some of the logging tools can be deployed while drilling, whereas others are post-drilling open hole imaging tools (Wang and Thagafy, 2017). The former typically have lower resolution (>1 cm), but detect more fractures as the there is no mud cake on the borehole wall yet that impedes the measurements (Al-Fahmi et al., 2023). In all borehole images, natural fractures appear as sinusoid traces contrasting with the resistivity or the acoustic signature of the host rock (Williams and Johnson, 2004). In this study, we focus on acoustic and optical borehole images only.

Boreholes “see” only a small portion of the rock or reservoir units they encounter (Howell et al., 2014; Ringrose et al., 2008). Consequently, the amount of discontinuities they intersect is far from the complete network which leads to large uncertainties when the borehole data is used for characterizing the reservoir (Khoshbakht et al., 2012). These uncertainties are primarily due to the geometry of the fracture network and the limited sampling size of the borehole. For instance, the spacing between fractures might be larger than the diameter of the borehole, which leads to poor overall sampling (Ortega et al., 2006). In addition, the 1D orientation of the well with respect to the 3D geometry of the discontinuities may also become an issue. In vertical wells, most of the sub-vertical discontinuities will be undersampled (Peacock and Mann, 2005).

Besides problems linked to the geometry of the discontinuity network, uncertainties are also related to the decisions made by the interpreter (human-induced) on the fracture picking from borehole images. Andrews et al. (2019) define uncertainties in handling geological data as being either objective (i.e., referring to technical errors) or subjective (i.e., related to interpreter’s perception and a priori knowledge). In borehole images, objective bias arises from either natural or technical challenges. On the natural side, fracture density is a key factor impacting borehole interpretation. Generally, the denser fractures are in a borehole, the more ambiguous the interpretation is due to overlapping features. On the technical side, it has been demonstrated that image resolution, drilling process, and quality of the borehole itself greatly influence the interpretation of borehole images (Lai et al., 2018; Lorenz and Cooper, 2020). A breakout structure may change the angle at which images are acquired by the logging tool, which causes local distortions and makes discontinuities less visible (Wedge et al., 2015).

Excellent studies exist on the topic of human-induced uncertainties (Bond et al., 2007, 2015; Andrews et al., 2019, 2024). Bond et al. (2007) introduced the notion of “conceptual uncertainty” (or subjective uncertainty sensu Andrews et al. (2019)) which is defined by the a-priori knowledge that geoscientists use to interpret a given dataset. These subjective biases are quantifiable but difficult to mitigate in an efficient way, as everyone with a geoscience education has them, regardless of their level of technical, applied or fundamental experience (Andrews et al., 2019).

Objective and subjective issues may lead to contradictory interpretations impacting engineering strategies deployed to appraise and exploit subsurface resources. For instance, in the West Netherlands Basin (WNB), a geothermal exploration well (NLW-GT-01) was drilled to evaluate the Triassic Buntsandstein, considered as a potential NFGR. The initial analysis of the resistivity image log allowed the operator of the log to recognize 300 natural fractures which identifies the Buntsandstein as heavily fractured. Later, Boersma et al. (2021) re-interpreted the same image log and identified only 58 natural fractures for the same interval. These discrepancies strongly affect the perception one can have about the potential of a targeted reservoirs and might lead to abusively appraising or discarding a certain geo-energy target.

2. Rationale

The present paper assesses the repeatability of fracture interpretation on borehole images and the related biases. Our study focuses on the Lower Cretaceous limestones of the Geneva Basin, which was penetrated by the well GEo-01 for geothermal exploration (see Fig. 1). From this well, 122 m of optical (OBI) and acoustic images (ABI) are available and allow the characterisation of the fractures affecting the targeted reservoir. The unique aspect of our case study lies in the independent interpretations of GEo-01 by five different operators with varying levels of experience.

Statistical data on discontinuities derived from BHI are classically used to constrain static subsurface discrete fracture network (DFN) models, which are instrumental in predicting fluid flow behavior of geothermal reservoirs (Li et al., 2024). Important parameters extracted from the BHI are fracture frequency and orientation of fracture sets, as these statistical parameters impact the degree of connectivity of the modeled fracture network. Therefore we focus on these two characteristics in this study.

First, we will describe the geological context of the geothermal campaign in the Geneva Basin. After this, we present the five different interpretations and outline how discontinuities were picked by the operators. Then, the technical and geological context of the well data is presented. Changes in quality and complexity of the image log are identified and the lithologies and deformation structures encountered by the well are described. The fracture interpretations of five different operators are compared based on fracture frequency and orientation and we highlight stratigraphic intervals of agreement and disagreement between operators. By identifying causes for the agreement/disagreement, we assess how technical and/or geological factors affect the degree of subjective bias in BHI-interpretations.

As there is no objective validation possible for the five independent BHI-interpretations, (e.g., core data), we consider all of them to be equally correct/incorrect. Hereby we do not aim to identify the best fracture interpretation for GEo-01, but focus on the impact of subjective bias on the interpretations, and eventually postulate recommendations aimed at mitigating the effects of this form of bias. To improve the quality derived from BHI in structural studies in general, we introduce the concept of controlled geological bias as a key element in the interpretation process.

3. Geothermal in the Geneva Basin, Switzerland

In 2014, the Canton of Geneva drew the contours of a new regional energy strategy and launched the GEothermie 2020 program, together with the University of Geneva and the Services Industriels de Genève (Moscariello, 2019). The objective of the program is to produce heat and electricity from geothermal energy in the Geneva Basin to reduce greenhouse gas emissions without resorting to nuclear energy. The large database from hydrocarbon prospection conducted between the ’60s and ’80s (including extensive well and 2D seismic data) allowed a re-evaluation of the architecture and the reservoir properties of the Cretaceous and Jurassic carbonates (Rusillon, 2017; Brentini, 2018; Clerc and Moscariello, 2020). Based on this knowledge, an exploration campaign began in 2017, which included the drilling of exploration well GEo-01.

3.1. The geothermal systems and the Lower Cretaceous aquifer

The currently targeted reservoirs in the Geneva Basin are located in the Lower Cretaceous carbonate sequence. The heat flow in the Geneva Basin is dominated by conduction (Moscariello, 2019), with an average geothermal gradient of 25–30°C/km (Chelle-Michou et al., 2017).

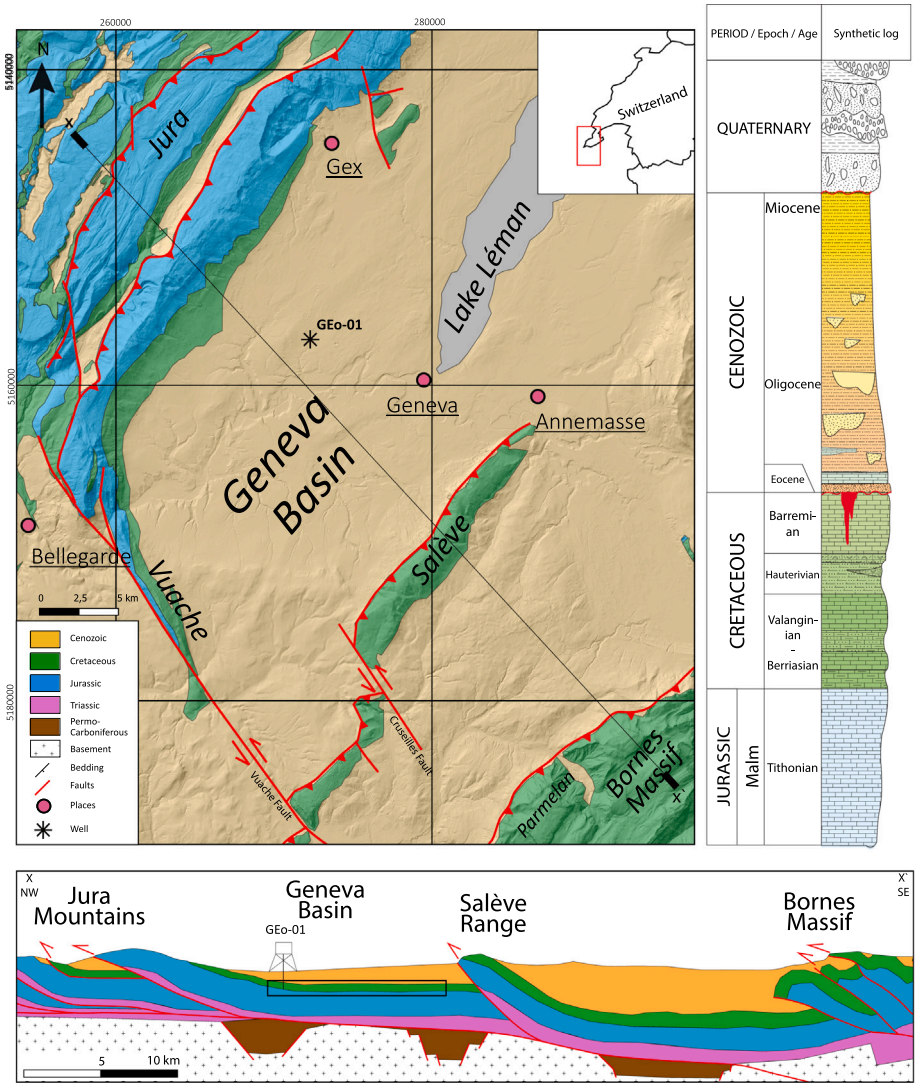


Fig. 1. Simplified geological map of the Geneva Basin and surrounding mountain ranges and outcropping regional faults (modified after Hupkes et al., 2026). The exploration well GEo-01 is located northwest of the city of Geneva. Right: synthetic log of the sedimentary succession in the Geneva Basin (after Moscariello, 2019). The Lower Cretaceous carbonate succession is targeted as a potential geothermal reservoir, due to the presence of natural fractures. 122 m of borehole images of this reservoir are obtained in GEo-01 (see Fig. 3. Bottom: cross-section displaying the structural position of the Geneva Basin between NW-verging Alpine thrusts. The black box indicates the targeted Lower Cretaceous carbonate rocks (modified after Bellahsen et al., 2014; Moscariello, 2019; Kalifi et al., 2021; Marro et al., 2023).

The recharge of the Mesozoic reservoirs is controlled by infiltration of meteoric water coming from the Jura Mountains (Guglielmetti et al., 2022). The Lower Cretaceous carbonate reservoir is the main target of this study and has been penetrated by the GEo-01 borehole drilled after the start of the 2018 exploration campaign. The Lower Cretaceous primary porosity and permeability are low, with average porosity values below 8% and permeability ranging from 0.001 to 10 mD (Rusillon, 2017). Additionally, the Lower Cretaceous rocks have high lithological variability due to the different sedimentological environments, but it is the secondary porosity and permeability from fracture networks and connected karst systems that create the potential of this reservoir (Moscariello, 2019). Flow rates from the Lower Cretaceous reservoirs in GEo-01 are 50 l/s at 34 °C (Moscariello, 2019) which is sufficient for the development of geothermal heat. These conditions qualify the Lower Cretaceous of the Geneva Basin as an NFGR.

3.2. Geological setting of the Geneva Basin

The Geneva Basin is located in the westernmost part of the Swiss Plateau. Geomorphologically, it consists of a low topographic zone of ca. 2000 km2 bounded to the NW by the Jura Mountains, to the SW by the Vuache ridge, and to the SE by the Salève mountain (Fig. 1). Guglielmetti et al. (2022) define four lithological units in the basin: the crystalline basement, the Permo-Carboniferous clastic sediments, the Mesozoic succession composed mainly of Triassic to Lower Cretaceous carbonate rocks, and the Tertiary clastic sediments. The general architecture of the basin is characterized by a gentle dip towards the SE, making lithological units shallower towards the Jura Mountains. The Jurassic and Lower Cretaceous rocks identified in the basin are outcropping in the surrounding reliefs, namely the Jura, Vuache and Salève.

3.3. Tectonic setting

The deposition of the Lower Cretaceous succession is associated with the opening of the Tethys Ocean (Scotese and Schettino, 2017). In the Geneva Basin, a shallow water carbonate platform was in place during the Late Jurassic (Moscariello, 2019). Shallow water conditions persisted during the Early Cretaceous (Do Couto et al., 2021). At the end of the Cretaceous and the beginning of the Cenozoic, the initial shortening phase of the Alpine Orogeny exhumed the Lower Cretaceous rocks. An

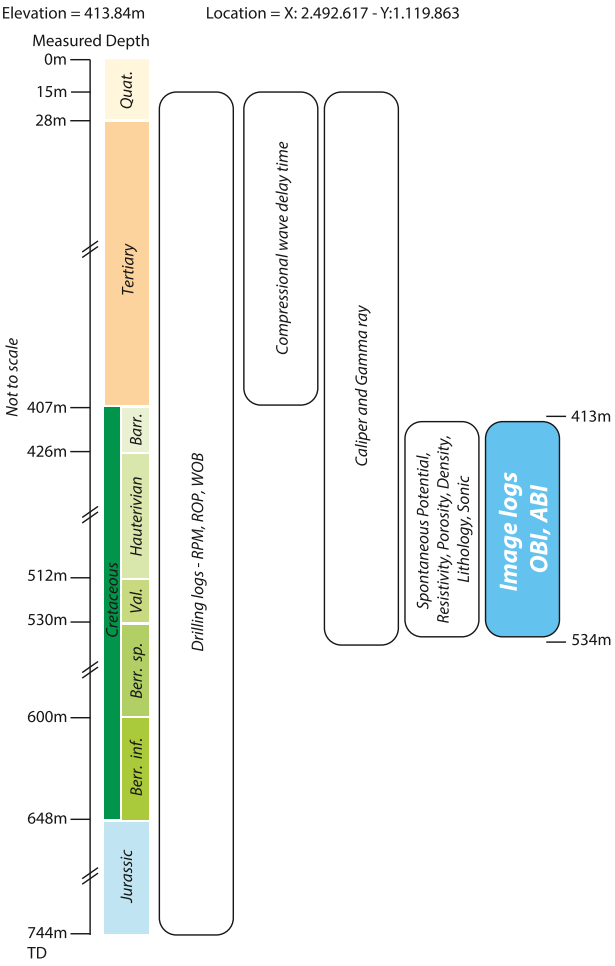


Fig. 2. Data from GEo-01, including interpreted stratigraphy and available geophysical logs. The optical and acoustic image logs (OBI and ABI respectively) are available from 413 m to 534 m (MD).

intense regional erosion (potentially removing up to 1.5 km of sediments (Schegg and Leu, 1998) occurred at that time and coincided with the intense karstification observed in the outcrops surrounding the Geneva Basin. The karsts are filled with the Eocene "siderolithique" deposits (Eruteya et al., 2024). While these karsts are highly heterogeneously distributed over the area (Guglielmetti et al., 2022), their presence is closely linked to an intense fracture and fault network affecting the Cretaceous and the Jurassic rocks.

The present-day architecture of the Geneva Basin is the result of the formation of the North Alpine Foreland Basin during the Alpine orogeny. This Miocene to Early Pliocene phase led to the decoupling of the Mesozoic sedimentary cover from the Variscan crystalline basement and Permo-Carboniferous clastic units through a décollement surface in Triassic evaporites (Sommaruga, 1999). The Alpine shortening was accommodated in the Geneva Basin by the emplacement of major fold-and-thrust belts (Jura and Salève mountains), and by multi-kilometre scale strike slip faults currently visible at the surface (e.g., Vuache range).

4. Geological and technical data of exploration well GEo-01

4.1. Geology of GEo-01

The GEo-01 well is located ~7.5 km WNW of the city of Geneva and has been drilled near-vertically to a depth of 744 m (Fig. 2). The Lower Cretaceous carbonate rocks are observed between 407 and 648 m depth (MD), with the interval between 413–534 m covered by the optical and acoustic BHI. The lithology was retrieved from cuttings acquired every 2 m during the drilling process. The analysis of the cuttings was completed with 117 thin sections providing details on microfacies and stratigraphic boundaries. The interval covered by the OBI log spans from Upper Berriasian to the Lower Barremian and includes four local sedimentary formations: the Chambotte Formation at the bottom, the Vuache Formation, the Grand Essert Formation, and the Urgonian facies at the top (Strasser et al., 2016). In this study, the interval covered by the OBI was divided into 19 sub-intervals corresponding to 14 distinctive lithologies (Fig. 3).

In addition to the lithological log and its description, GEo-01 has been logged with calliper, gamma ray, density, spontaneous potential, and sonic geophysical tools (Fig. 2). Hydrocarbon indications (oil and gas shows, gas concentration) and hydrogeological information (water flow, conductivity, pH, and temperature) are also included in the well logs.

4.2. Quality of the borehole images for fracture interpretation

To assess whether the condition of the BHI is suitable for reliable interpretations, we conducted both a qualitative and a quantitative investigation of the images. The qualitative approach focused on evaluating the continuity of the sinusoids, the brightness of the background, the presence of voids and breakouts, the sharpness of the image and the contrast of the image (see Fig. 4). For each parameter, a score based on a determination key was attributed (Fig. 4). The higher the score, the lower the quality of the OBI. The quality of the OBI was assessed by Bruna and Hupkes independently. The scores were then compared to rank the quality of the BHI at the meter-scale (Fig. 5A, 1 and 2). The average score obtained by Bruna was 10.3, while Hupkes obtained an average score of 11.8. We took the average of these two scores (11) as the threshold separating good from bad quality intervals (<11) and >11 respectively). When the two operators agreed on the quality of the images, this interpretation was retained in a composite quality log, whereas when the interpreters disagreed, the quality assessment was excluded from the composite log (Fig. 5A–Q).

The quantitative approach is based on the image complexity map (OBI-ICM) functionality in WellCAD™. This functionality is based on the work of Wedge et al. (2015) who focused on optical parameters of the BHI to map the completeness and the amount of sinusoids present in the image. In this method, the sinusoids are detected using the phase-symmetry method which ignores contrasts in the background image. This approach is therefore less complete than the qualitative one, providing only a quantification of the (partial) completeness of the sinusoids in a considered session. The complexity mapping returns a normalized score where 0 means that the image interval is simple, and 1 means it is complex. Applying this method to the BHI of GEo-01, we obtain an average complexity score of 0.57. We use this value as the threshold separating a simple (<0.57) and a complex (>0.57) interval of the BHI and synthesize these results into the composite complexity log (Fig. 5B).

4.3. Five independent BHI fracture interpretations

Fractures in GEo-01 have been interpreted by five different operators independently, in different locations and/or at different times. Information on the different interpreters and the projects they worked on is stated in Table 1. Four interpreters used WellCAD (https://www.alt.lu/) and one used Techlog (Schlumberger). For the sake of harmonizing datasets, the dataset acquired in Techlog was imported into WellCAD.

The classification of fractures on image logs is based on the morphology of acoustic and electric properties. Open/shear fractures appear transmissive/dark on the OBI and are low amplitude/dark on the amplitude log. Veins appear reflective/bright on OBI and do not show up on the amplitude logs, as the contrast between infill and host rock is too low. Induced fractures appear transmissive/dark on the OBI and are low amplitude/dark on the amplitude log. They often appear irregular and asymmetric, with high dip angles. They are often associated

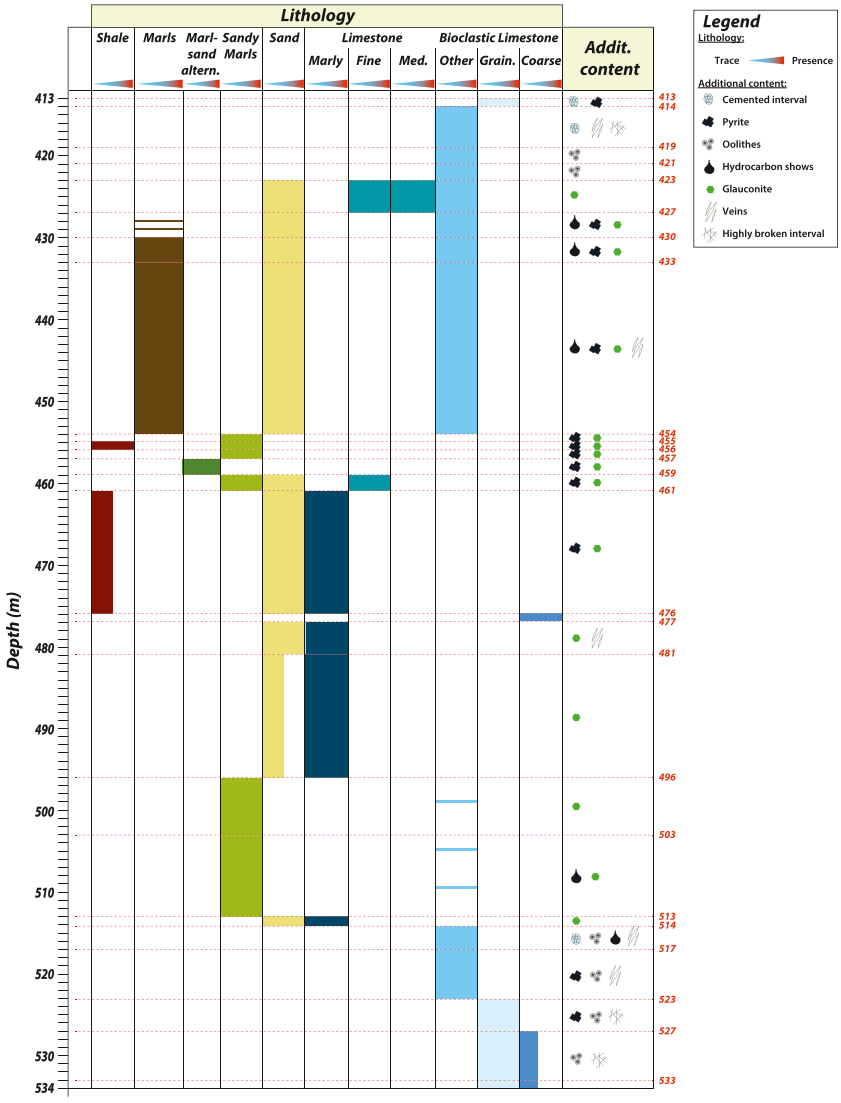


Fig. 3. Lithology of GEo-01 over the interval covered by the borehole images (413–534 m). The log is based on the lithological report and on the master log information, and lithological intervals have been divided as described in these documents. In each distinct lithological interval (highlighted by red dashed lines) multiple lithologies can be present. Sometimes (i.e., between 461–476 m) a trace of a certain lithology is described (here shales). Abbreviations: altern. = alternations, Med. = Medium, Grain = Grainstone. The log also includes indications of remarkable minerals and mineralization, traces of hydrocarbons, specific grain types (ooliths) and specific fractures described in cuttings.

with incomplete and repetitive sinusoids (Chatterjee and Mukherjee, 2023). The induced fractures are discarded from the datasets before the comparison of the different interpretations.

Two interpreters (KL and MD, see Table 1 also classified bedding planes. The definition used by these operators to define the bedding planes is a repetition of similarly oriented sinusoidal shapes within short interval (typically <1 m). They can appear both reflective and transmissive on the OBI, depending on the filling material. The operators found that the beddings are shallow dipping (<30°) in the top and bottom sections of the BHI, indicating that these areas are relatively undeformed. An increase in bedding dips (up to 56°) is observed in the middle section of the log, suggesting that this zone is affected by deformation, in the form of a fold, potentially related to a fault (Lo, 2019; Doesburg, 2023).

5. Investigating consistency of fracture frequency and orientation in GEo-01

5.1. Picking features in GEo-01

We compiled the number of open/shear fractures, mineralized fractures and beddings identified by the five independent interpreters in GEo-01 (Table 2). These picks form the basis for the frequency and orientation analyses. Three categories were defined based on this dataset:

- All features = open fractures, mineralized fractures and beddings
- Open features = open fractures and beddings (picked by MD, KL, GGE and MK only)
- Mineralized = mineralized features only (picked by all five interpreters)

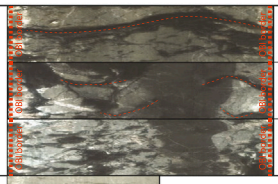
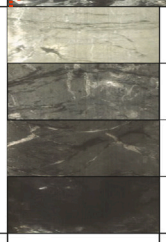
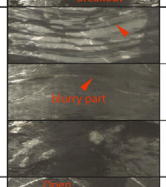
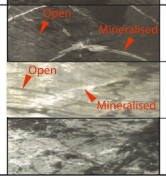
Param.	Example from GEo-01	Determination key	Score
Sinusoids continuity		Complete sinusoids	1
		Partial sinusoids	2
		Sinusoids are fragmented and difficult to trace	3
Dominant rock colour		Dominantly white	1
		Dominantly grey	2
		Dominantly dark grey	3
		Dominantly black	4
Voids		Absent	1
		Present	2
Breakouts		Absent	1
		Present	2
Sharpness		The image is very clear (sharp enough to see the sinusoids)	1
		Sharpness of the image decreases (parts less in focus than others)	2
		The image is blurry	3
Contrast		Distinction between mineralised and open features is possible	1
		Distinction between mineralised and open features is difficult	2
		Distinction between mineralised and open features is impossible	3

Fig. 4. Evaluation of the 'quality' of the borehole image in GEo-01.

Feature frequency was computed using a 1-meter moving window. For the categories 'all' and 'open', the analysis includes four interpreters only, while for 'mineralized', it includes all five. To quantify variability among interpreters, we calculated the minimum and maximum pick densities per meter and used these to construct an envelope encompassing the full range of individual interpretations (Fig. 7). While the trend of interpretation shows a first order consistency between interpreters, the absolute value of pick counts shows differences reflecting interpretation uncertainty.

5.2. Agreement on fracture frequency: impact of technical and geological factors

To investigate the influence of image quality, complexity and lithology on picking frequency, we first constructed cumulative frequency curves for features picked in GEo-01. Changes in slope at specific inflection points reflect shifts in the consistency of feature picking behavior which could correspond to intervals of increased agreement or disagreement. To identify the depth at which these transitions occur, we computed the derivative of the cumulative frequency of each interpreter and averaged these gradients across interpreters. Local extrema in the average gradients were interpreted as transitions in interpretation consistency.

The intervals of consistent picking behavior were studied separately for the open and vein populations. Open features show seven intervals of consistent behaviors, bounded by the black dashed lines, whereas the veins are divided into thirteen (Fig. 8).

To investigate the degree of agreement or disagreement between interpreters within each identified interval, we calculated pairwise differences in picked features per meter across all interpreters. The result is a bar plot where absolute picking differences are computed (Fig. 9). The intervals as depicted by the cumulative curves (Fig. 8) are drawn on the bar plot. Below, we investigate how the agreement/disagreement of interpreters is related to the geology encountered by the borehole and the technical quality of the BHI.

5.2.1. Open feature analysis

Interval with agreements. The highest agreement is in intervals 1, 3 and 6, where the pairwise interpreter differences for open features are the lowest. Intervals 1 and 6 are dominated by bioclastic limestone. In interval 1, the mean difference between interpreters is 2.8 features. Although poor image quality and high complexity restrict the number of identified features to 5, interpreters consistently identified the same number of counts. Toward the base of the interval (from 420–428 m), where image complexity decreases and quality improves, feature counts increase to 10 without introducing additional disagreement.

Interval 6 shows low differences between interpreters (average of 4 features). This interval is composed of a bioclastic limestone with grainstone texture. In interval 6, the complexity is low (88% simple), and image quality is good over 40% of its length. Despite the high number of features picked (up to 18), interpreters' disagreement remains limited.

Interval 3 similarly shows low disagreement between interpreters but has a different lithology, as it is dominated by marls and sand. 78% of the

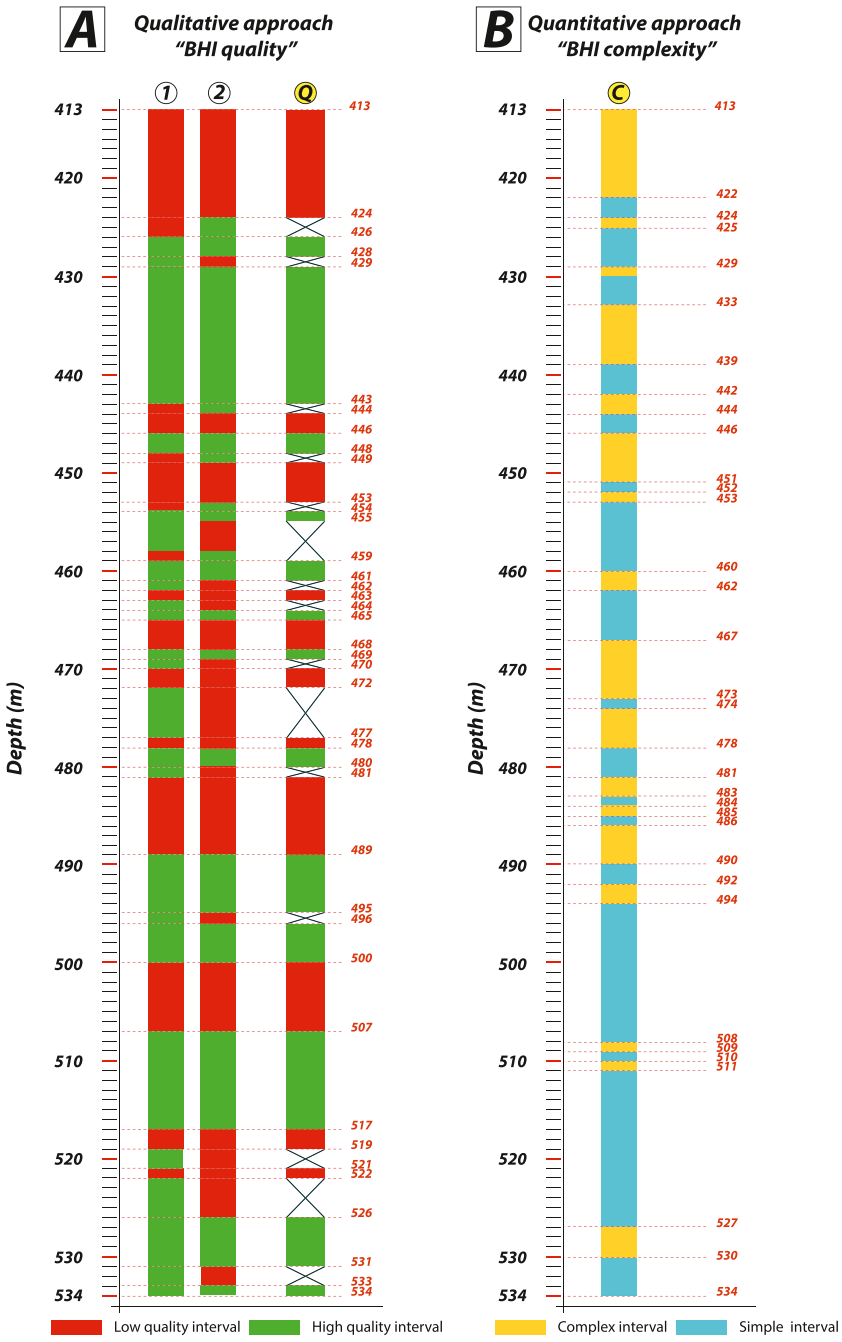


Fig. 5. Quality and complexity analysis of the BHI interval of GEo-01. A) Qualitative approach based on the comparison of the quality analysis of Bruna (1) and Hupkes (2). Intervals of agreements are kept in a composite quality log (Q). B) Quantitative approach based on the work of Wedge et al. (2015) implemented in WellCAD. The log (C) is the composite complexity log.

interval is classified as simple and 33% has poor image quality. There is a remarkable increase in differences at lithological transition occurring at 455 m.

Intervals with high disagreement. Higher disagreement was consistently observed in intervals where marls, sands, glauconite, or hydrocarbons shows were present (Intervals 2, 4, 5 and 7; see Fig. 10). In Interval 2, a marked lithological transition at 430 m from bioclastic limestone to marl and sand containing glauconite and hydrocarbons produced one of the strongest divergences between interpreters. Although image quality is high in this interval, the complexity remains elevated (59%). In this section, interpreter GGE systematically disagrees with KL and MD. KL and MD disagree the most with MK between 428 and 439 but converge deeper in the same interval. The couple GGE-MK remains largely consistent throughout the interval.

Interval 4 comprises marly limestone and sandy units. 57% of the interval is complex, and at least 41% of it has poor image quality. Although interval 4 has the same average difference as interval 6 (4 picks), it contains several pronounced sub-intervals of divergence that justify its inclusion in the high-difference group. Localized mismatch spikes (>6 features difference) occur at lithological transitions, such as at 461–462 m, 477–478 m. Additional disagreement clusters occur at 468–471 m (complex and poor quality), 479–480 m (simple), 490–492 m (simple), and 494–495 m.

Table 1
Summary of BHI interpretations of GEo-01. Abbreviations: UniNE is University of Neuchâtel; UNIGE is University of Geneva; TUD is Delft University of Technology.

Interpreter	Acronym	Location	Degree	Supervis.	Software
Koumrouyan (2019)	MK	UniNE	MSc	External academic supervisor	WellCAD
Lo (2019)	KL	UNIGE	MSc	A. Moscariello (academic)	Techlog
Services Industriels de Genève (2020)	GGE	Geneva, Switzerland		Industry Consultant	WellCAD
Barreiros Jorge (2023)	SJ	TUD	MSc	P-O. Bruna, G. Bertotti (academic)	WellCAD
Doesburg (2023)	MD	TUD	MSc	P-O. Bruna, J. Hupkes, G. Bertotti (academic)	WellCAD

Table 2
Overview of number of picks per type for all interpreters.

	MK	KL	GGE	MD	**SJ**
Open/Shear	803	407	573	607	
Mineralized	161	152	73	213	127
Bedding		488		195	
Total	**964**	**1047**	**646**	**1015**	**127**

Interval 5 consists of sandy marls with thin bioclastic beds, glauconite and hydrocarbon traces. It exhibits a very high disagreement level (average of 5.5 picking difference) despite the simplicity of the image in the interval (88%) and its good quality (59%). In this interval, GGE, KL and MD diverge from all other interpreters. In contrast, MK tends to agree with KL and MD throughout.

Interval 7 is dominated by coarse and fractured bioclastic limestone and produces the largest difference across the entire dataset (mean difference of 10.6 picks). Compared to interval 5, GGE aligns more closely with KL and MD. MK, KL and MD tend to disagree with all other interpreters.

Synthesis. Lithology appears to have a strong control on interpretation consistency. Intervals dominated by bioclastic limestone without glauconite (1 and 6) yield the lowest interpreter differences. In contrast, intervals characterized by marls and sands, and by the presence of glauconite or hydrocarbons (2, 4, and 5) consistently show higher disagreement between interpreters.

Intervals 3 and 7 deviate from these lithology-based trends. While interval 3 is composed of marls and sands, the markedly low complexity of the image in this interval leads to a low disagreement between interpreters. Interval 7 stands out for its high disagreement between interpreters in a coarse bioclastic interval. In this interval, the results suggest that localized intense fracturing combined with a poor image quality appears to override the stabilizing effect that bioclastic lithologies exert in other intervals.

There is no consistent pattern in the agreement/disagreement of interpreter pairs. Overall, GGE is in disagreement the most, consistent with their lower total number of picks (646) compared to the other interpreters. However, in intervals 2, 5 and 7, marked differences are also observed among the other interpreter pairs.

5.2.2. Mineralized features

Intervals with agreement. The intervals of highest interpreters' agreement, defined by an average difference of < 2 picked features, are intervals 8, 13, 14, 16, 18 and 19. Interval 8 is in bioclastic limestone with high image quality and low complexity, conditions that promote consistent identification of mineralized features.

Intervals 13 and 14 consist of marly limestone with siliciclastics and glauconite. Both intervals are predominantly simple (60%), but image quality differs markedly: at least 40% of interval 13 has poor image quality, whereas most of interval 14 (at least 80%) is of good quality. Despite this contrast, both intervals maintain low interpreter variability.

Intervals 16 consist of sandy marls with glauconite and traces of hydrocarbons. While image quality is poor in the upper part (500–507 m), the interval is overall simple (90%) which likely contributes to the agreement.

Intervals 18 and 19 occur in bioclastic limestone. These intervals have low image complexity. Interval 18 is dominated by poor image quality (71%), whereas at least 50% of the interval 19 is deemed to be of good quality. Notably, 43% of Interval 18 is highly cemented, which may enhance vein visibility and favor agreement.

Intervals with disagreement. The intervals of highest disagreement between interpreters are 9, 10, 11, 12, 15, 17 and 20. They have an average difference in picked features >2. Interval 9, the longest, is marl-dominated with hydrocarbon shows. Image quality is generally good (at least 58%), and mostly simple (54%). Most disagreements occur between 439 and 449 m. In this sub-interval GGE disagrees with MD, MK and SJ and MD disagrees with MK and SJ. KL is largely consistent with the other interpreters. Intervals 10, 11, 12, 15, and 17 occur in sandy marls, marly limestones and sand units containing glauconite. Lithological transitions occur within interval 10 and at the top of interval 15. The image quality is poor in intervals 10, 11, and 12, whereas it is good in intervals 15 and 17. In all these intervals the image is mostly simple. In interval 10, GGE and KL both disagree with MD and MK. In interval 12, the highest difference occurs between GGE and KL, MD and MK. We also observe that KL disagrees with MD and MK and that MK disagrees with SJ and MD. In interval 15, the most important disagreement is between GGE and KL. In intervals 11 and 17 the disagreement is more diffuse.

Interval 20 occurs in a coarse bioclastic limestone. The image in this interval is mostly complex (67%) but is of good quality.

Synthesis. Four intervals lacked identifiable mineralized features over the whole interpretation dataset (413–425 *m*, 428–431 *m*, 483–491 *m*, and 519–524 *m*). These intervals show consistently poor image quality and high complexity. Bioclastic limestone is the dominant lithology and, despite the presence of veins in cuttings, mineralized features are not picked by the interpreters on the BHI. This suggests that lithology itself, rather than image attributes alone, may hinder vein detection in such settings.

Marl-rich intervals (9, 10, 11, 12, 15, 17) show the highest interpreter variability, particularly at lithological transitions. Although these intervals are generally characterized by low image complexity, this does not translate into improved agreement among interpreters. Image quality does not seem to provide a consistent pattern either: intervals 9, 15, 17 are of high quality whereas 10, 11, 12 are dominantly of poor quality, yet both groups display comparable disagreement levels.

Intervals 13 and 14 occur in marly limestone with sands showing consistent agreement, despite lacking a specific combination of technical parameters that could account for this behavior. Bioclastic limestones yield few or no veins, likely due to weak imaging contrast rather than issues with image quality or complexity. The intervals occurring in this lithology (8, 18 and 19) show high agreement level.

Across all intervals, GGE and KL tend to consistently disagree with MK and MD indicating a systematic difference in picking strategies rather than level specific effects.

5.3. Agreement on fracture orientation

To assess how well fracture sets can be defined based on borehole image interpretations, we compare the orientation of the fractures picked by the different operators in GEo-01 in two ways. To analyze angular differences between features, poles to the planes of all features are plotted (see supplementary materials for stereoplots of the poles), and they

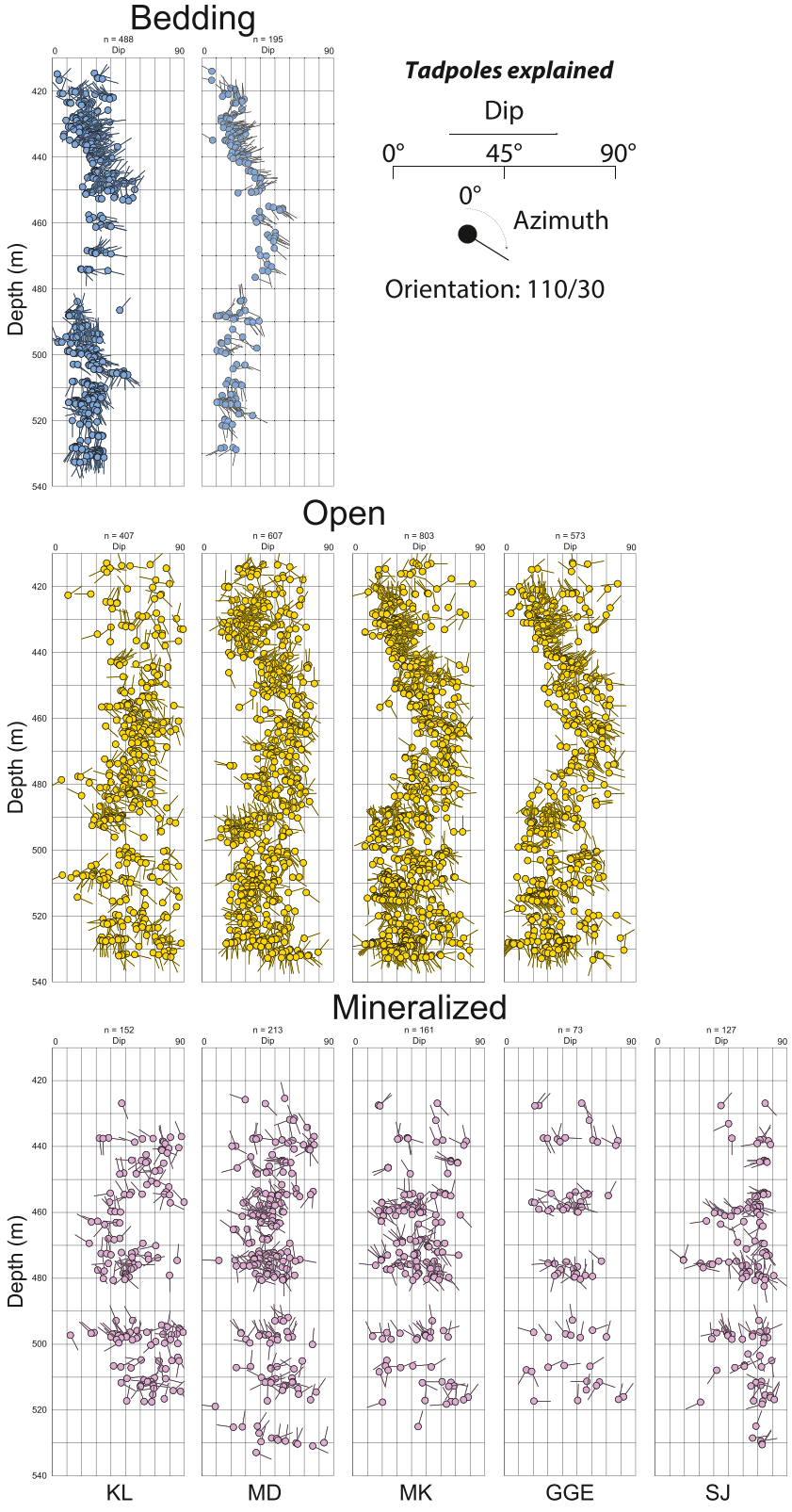


Fig. 6. Picked features on the BHI of GEo-01 by five independent interpreters plotted as tadpoles versus depth. Each feature type (bedding, open and mineralized) is plotted separately. Two interpreters picked bedding on the BHI (KL & MD). SJ only picked mineralized features. The total number of features per interpreter is summarized in Table 2.

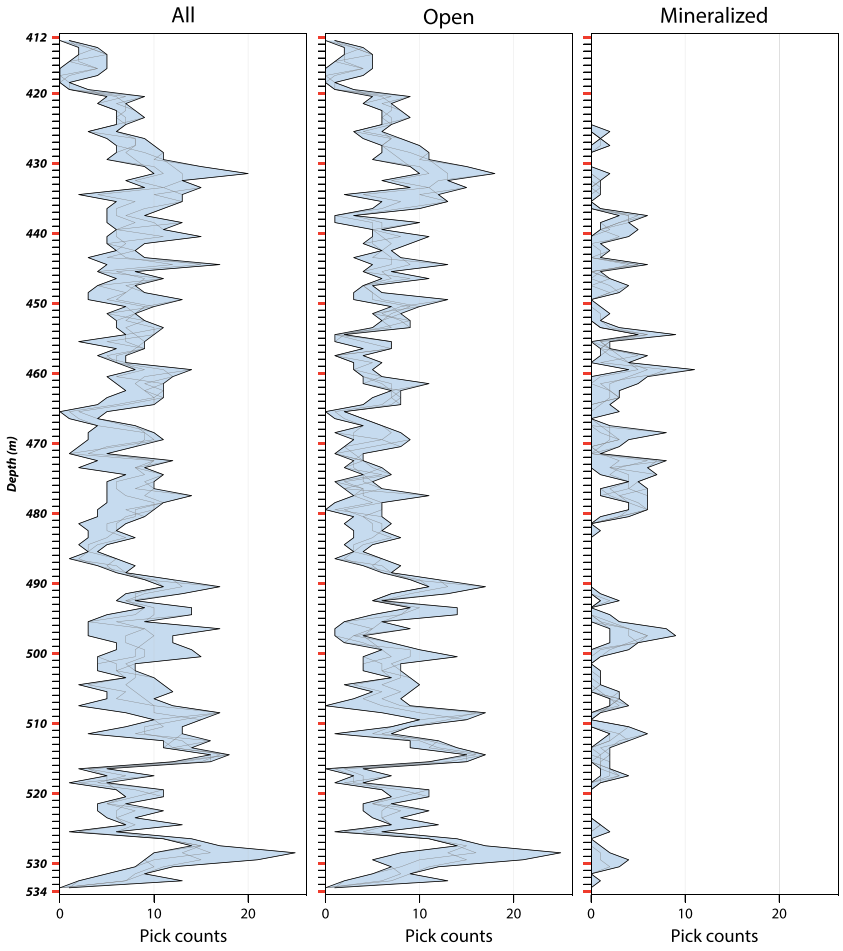


Fig. 7. Comparison of the pick counts for the three feature populations. The individual interpretations are represented in grey and included in the envelope (blue). Minimum and maximum values are represented by the borders of the envelope.

are subsequently averaged per meter, similar to the frequency analysis. The angular dispersion is then calculated by taking the angle between the two poles of different operators that are the farthest away from each other.

As the frequency analysis (Section 5.2 has shown in some intervals there is a large variability in the number of features picked. Averaging the orientation per meter might obscure agreement among interpreters on individual features picked on the BHI. To identify these features, the assumption is made that if all operators picked a feature at the same depth of the log (within a 1 cm margin), they in fact picked the same feature (Fig. 11). The pole vectors to the features picked at the same depth are calculated and the standard deviation of the poles from the average orientation is used to decide if the operators agree on the orientation or not. We consider a deviation of 15° as agreement between interpreters; if the deviation is higher, we consider this feature unreliable for defining fracture sets in the BHI. This procedure is repeated to filter for features on which all but one of the operators agree to assess if there is one operator consistently off.

The analyses are applied to the open features and mineralized features separately. The results are plotted versus depth, to locate intervals of agreement and disagreement on the orientation between interpreters. These intervals are compared with the intervals defined by the frequency analysis (see Section 5.2).

5.3.1. Results

The angular dispersion of the averaged orientations of the open features shows a variability of agreement along the well (Fig. 12). Overall, the dispersion is larger than 15° for most of the log (83 out of 122 meters), with most spikes in the curve locate between 450 and 485 m. Of al the individual features interpreter by the four interpreters, 79 have a similar orientation (Fig. 12), which is 12% of the smallest dataset (646 GGE, Fig. 6). The gap between these intervals roughly coincides with the spikes in the dispersion plot. The total number of features on which three operators agree is significantly higher with 151 features (Fig. 12). There is not a single operator consistently off – this dataset is comprised of different combinations of three out of the four operators. The features are more distributed over the whole depth of the log than the features on which all agree, but the majority are found in the interval between 420–450 m.

Also for the mineralized features only the angular dispersion varies along the full image log (Fig. 13). The dispersion is below 15° for only 8 m of the log, indicating that on average the five interpreters do not agree on the orientation of the mineralized features. This is confirmed when looking at the individual feature comparison; there are 3 mineralized features on which all five operators agree (Fig. 13), which corresponds to 4% of the dataset with minimum picks (73, GGE). The number of features increases for the cases where four and three interpreters agree (6 and 21 respectively), and they do not cluster in clear intervals along the log.

5.3.2. Synthesis

There is little agreement between operators on the orientations of the interpreted open and mineralized features. For the open features, the highest agreement between operators is mainly at the top (428–455 m)

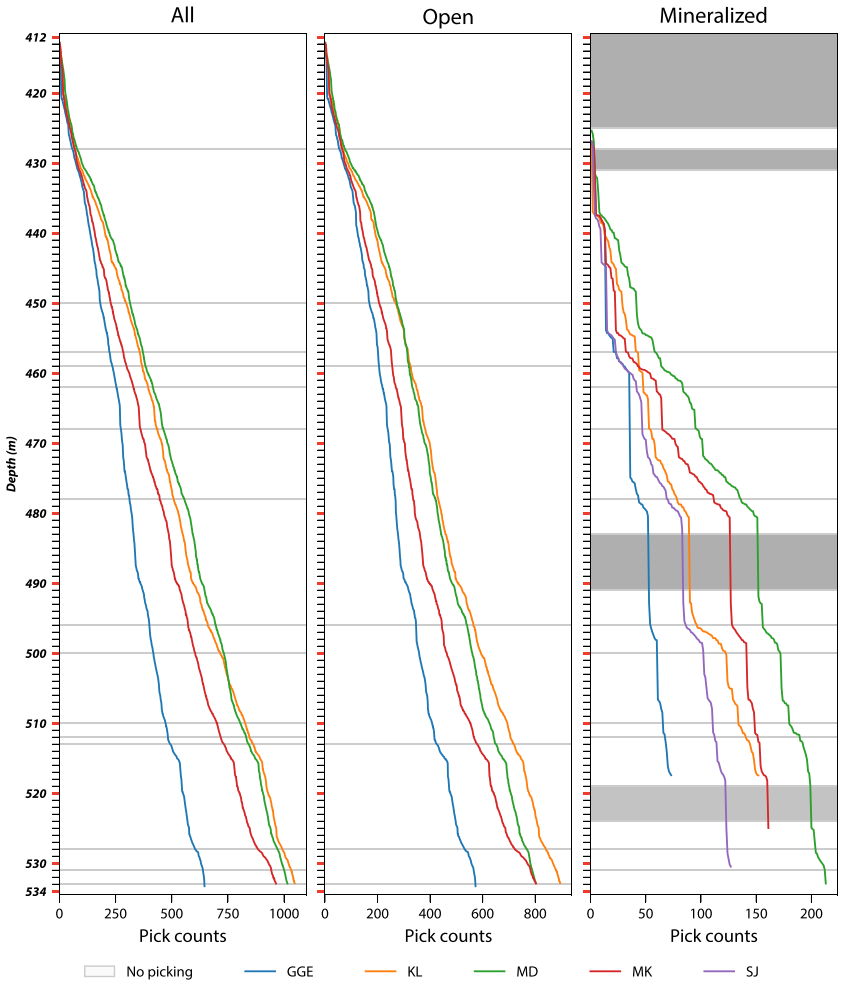


Fig. 8. Cumulative picking frequency plots presenting the intervals of consistent picking behavior (black dashed line). A) Cumulative frequency plot of all features. B) Cumulative frequency plot for open features. C) Cumulative frequency plot for mineralized features. Dark grey bands indicate intervals where no mineralized features are picked at all.

and to a lesser extent at the bottom section of the log (485–533 m). The former interval coincides with interval 2 of the frequency analysis, an interval which has little agreement on the frequency (Fig. 9). The latter overlaps with intervals 4 to 7, of which only interval 6 showed more consistent frequency interpretation (Fig. 9). The low number of agreed mineralized features does not allow for any kind of correlation with the intervals defined in the frequency analysis. This suggests that the causes for divergence in frequency interpretation such as lithology do not have the same impact on orientation interpretation.

On the other hand, there seems to be a negative correlation between the agreement on orientation of open features and the increase in bedding dip between 440 and 480 meters as observed by KL and MD (Fig. 6). It is in this interval where agreement between interpreters on the orientation of the picked open features is the lowest, which suggests that features picked in intervals affected by some sort of deformation will have a higher uncertainty regarding their interpreted orientation compared to intervals where the bedding is consistently low-dipping.

The results show that defining the orientation of fracture sets on BHI is far from trivial. There is very little agreement between different operators on the orientation of features, and the interpretations are likely not reproducible and are affected by subjective bias. The impact of technical and geological factors on the interpretation of orientation of features is not the same as for the frequency Table 3.

6. Discussion

6.1. The reliability of BHI interpretations

A common method to assess how well fracture interpretation on BHI represents the true amount of fractures in the subsurface is by correlating picks on the image logs with fractures observed in core. Several studies provide guidelines for obtaining reliable BHI interpretations, and the results of the core-to-log correlation are extended to cases where there is no core available. For instance, it has been demonstrated that if sinusoids on the image logs are near continuous, there is a high chance that they can be correlated with fractures observed in the core (Fernández-Ibáñez et al., 2018; Playton et al., 2025), making these picks on BHI more reliable. Other studies found that open, sub-vertical fractures on BHI have a high correspondence in core, in contrast to filled fractures, low-angle fractures and dissolution surfaces such as stylolites, due to resolution limitations of the images and/or lack of resistivity contrast between fracture and matrix (Laubach et al., 1988; Khoshbakht et al., 2012).

However, these studies did not investigate the reproducibility of the BHI interpretations, regardless of whether features on BHI can be correlated with the core or not. Typically, in exploration projects, there is only one operator who interprets all the BHI logs, which makes the interpretation prone to recurring bias. Bourke (1992) investigated the repeatability of picking sedimentary features on BHI and they concluded

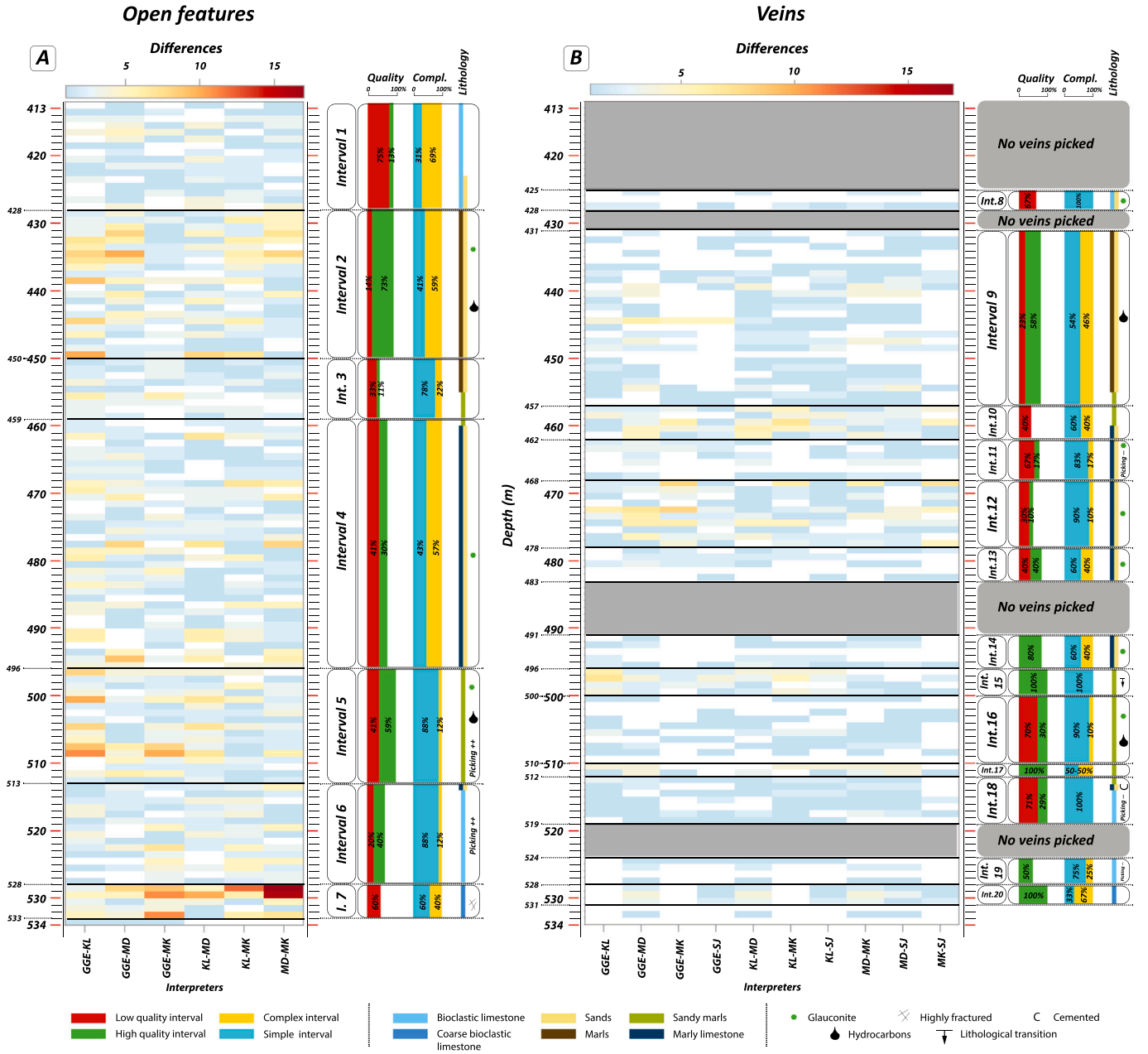


Fig. 9. Pairwise differences between interpreters for: A) open features (including beddings and open/shear fractures) picked by four interpreters only; B) mineralized features picked by all five interpreters. The intervals identified on the right-hand side of the figures come from the cumulative picking plots (Fig. 8). The column at the right end of each figure summarizes the image quality (expressed as percentage; the sum of poor and good quality can be below 100% when discrepancies between quality interpretations arise, see Section 4.2 and Fig. 5) the complexity, the dominant lithology and identified particularities such as glauconite, hydrocarbon shows, intense fracturing, cementation or lithological transition within a given interval. The blue values correspond to low differences between the two considered interpreters and red values denote high differences. The determined intervals are compared based on agreements and disagreements with technical (quality/complexity Section 4.1) and geological (lithology Section 4.2) controlling factors to assess their influence on picking behavior. The analysis is divided into intervals of high agreement (mainly blue) and intervals of disagreement (mainly yellow and red). This approach provides a systematic quantification of interpretation consistency as a function of lithology and borehole image complexity/quality for both feature populations (open features and mineralized features).

that BHI can be reliably used for paleocurrent analysis, but similar research has not been carried out on BHI of fractured intervals.

The results of the present study show that the variability of fracture frequency and orientation among different interpretations of the same BHI is such that deriving statistical fracture parameters for reservoir characterization is far from trivial. We demonstrated that there are technical (quality and complexity of BHI, see Section 5.2) and geological (lithology and structures see Sections 5.2 and 5.3) parameters that impact the reproducibility of BHI-interpretations. This implies that guidelines based on core-to-log correlations alone are not sufficient to guarantee repeatable BHI fracture interpretations. Considering these potential issues before starting to interpret the wellbore is therefore of key importance to increase the repeatability of the interpretation and to subsequently minimize the impact of uncertainties in the subsurface domain.

On the technical side, Bourke et al. (2014) recognize the progress made in availability and overall improved quality of subsurface data in various geological contexts. However, these authors warn that users

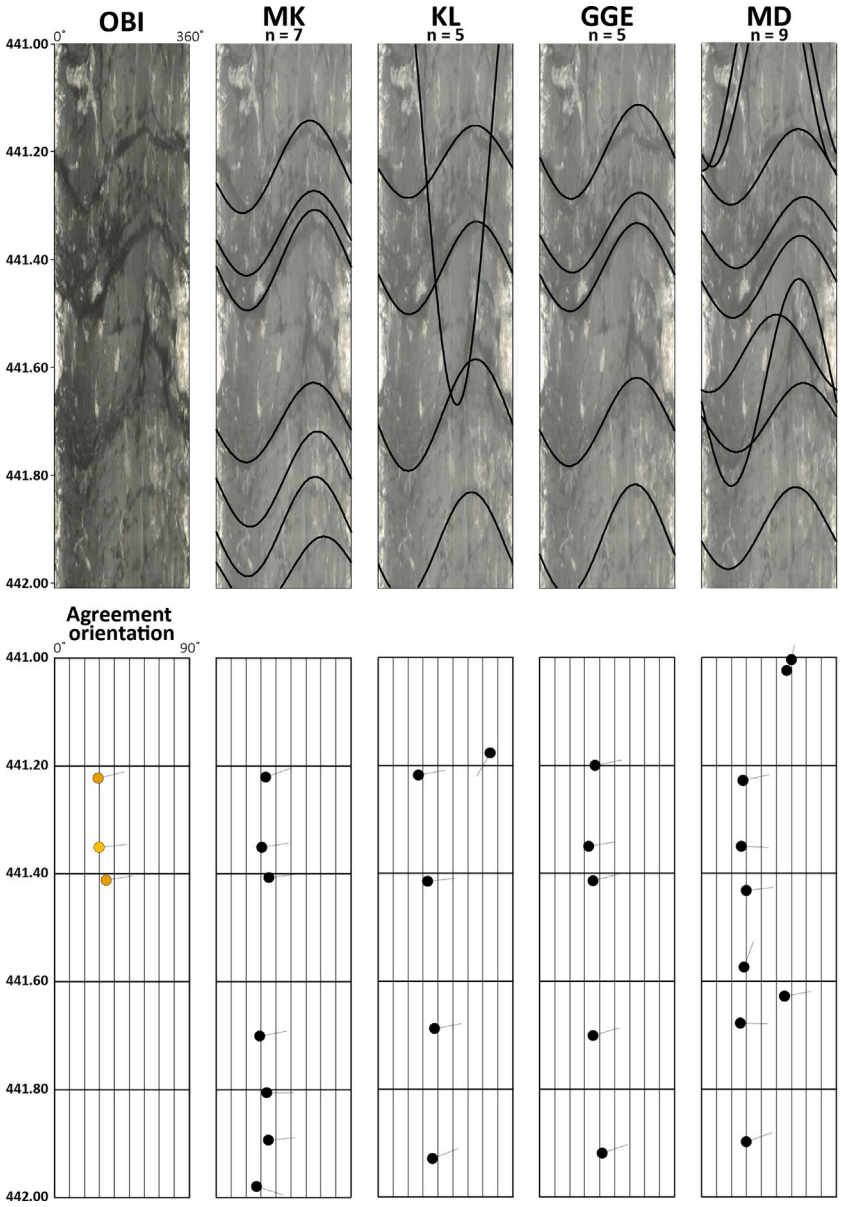


Fig. 10. Example of different interpretations of a 1-meter interval in a sand-marl dominated section, part of interval 2 (see Fig. 9), with OBI image as background (scale 1:10). Below, tadpoles of each interpretation are plotted. On the bottom left, the picks on which interpreters agree are plotted, following the procedure described in Section 5.3. Differences in frequency may have different causes. Some interpreters are conservative in the number of picks: for example, at 441.40 m depth, KL picks only one feature, whereas the others interpret two. At the same time, KL and MD pick steeper features than MK and GGE, potentially related to the scale at which they interpret the image. Although sinusoids appear to have the same shape at the displayed scale, the depth at which they are interpreted varies. All interpreters for example pick a similar feature around 441.70, but as the feature does not make a perfect sinusoid on OBI, interpreters pick the feature at different depths (441.70, 441.67, 441.68 and 441.70).

may misperceive technical advances, often treating these cutting-edge data as trustworthy by default. The authors estimated that more than 40% of borehole images contain objective errors, such as corrupted data formats, incomplete datasets or logging tool issues, which might result in misleading interpretations. Therefore, they encourage users to conduct a thorough control of the quality of borehole images before the interpretation. In our study, we quantified the impact of complex and/or poor-quality intervals of the BHI on the convergence of interpretation (Fig. 9) and show that image quality and complexity play a subordinate role in divergence of frequency interpretation. However, when combined with unfavourable lithological intervals (i.e., marls), image quality and complexity do exert control on the divergence of interpretations. Therefore, we recommend in future interpretations to start with a manual or automated inspection of the quality and complexity of the borehole image before picking fractures, to highlight upfront intervals where the interpreters are likely to encounter difficulties. This pre-processing could then be seen as a necessary quality control check potentially leading to more aligned interpretations.

6.2. Integrating a controlled geological bias to improve borehole image interpretation

On the geological side, we demonstrated the influence of lithology and structural attitude (tilt of the bedding) on the interpretation of the BHI of the Lower Cretaceous carbonate rocks in the Geneva Basin. We suggest here using the results of this study, and beyond to propose the

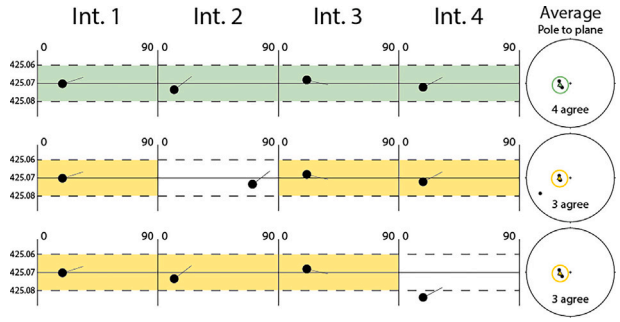


Fig. 11. Method applied to compare individual feature orientations between different interpreters. Features that are picked at the same depth (with 1 cm margin) are considered picks of the same feature on the BHI. The different features are plotted as poles on a stereonet. If all poles are within 15° from the Fisher mean vector (small circle in the stereoplot), they agree on the orientation of this feature and this pick is represented in the bar plots of Fig. 12.

introduction of a controlled geological bias prior to the interpretation of borehole data.

Fracture drivers such as faults and folds can be used as a priori knowledge to constrain the expected type of fractures intersected in a borehole. Several outcrop studies propose that there is a link between deformation structures and related fracture distribution. For example for faults, scaling relationships between fracture density and distance to fault and fault size have been proposed (Caine et al., 1996; Micarelli et al., 2006; Choi et al., 2016; Torabi et al., 2023; Mayolle et al., 2023). The same applies to fold structures. Ameen and Cosgrove (2000) studied buckle and forced folds and reviewed the type and spatial distribution of fractures within these structures. More recent studies (Lucca et al., 2023; Watkins et al., 2015) have continued to enrich the knowledge about fracture patterns in fold structures increasing the predictive capacity in both outcrop characterization and in the subsurface.

The outcomes of these works are particularly relevant for the introduction of a controlled geological bias in BHI interpretation. Significant folds and faults (in the order of 10 to 100's m) can be recognized in seismic data. Therefore, one can evaluate before starting to interpret a BHI, the likelihood of encountering fractures related to these structures. Fracture orientations and potentially fracture intensity can be anticipated at the depth intervals where the fold/fault intersects the borehole. Any fracture falling outside of the expected model would be temporarily discarded, and a different geological concept/fracture-driver will be needed to contextualize the occurrence of these initially discarded features. A similar approach can be followed for folds where initial simple models can be considered to predict fracture patterns and to which complexity can be subsequently added if needed (Watkins et al., 2015). The impact of different drivers on the overall fracture network can be discriminated in this way, which will not only improve the BHI interpretation, but also increase its value for extrapolation to reservoir-scale (see, e.g., Hupkes et al., 2026).

6.3. A protocol to reduce subjective bias in interpretations

The integration of a controlled conscious geological bias before interpreting BHI also has the potential to reduce subjective bias. Bond et al. (2007, 2015) define three classic types of bias in interpretation of geoscientific data: the anchoring, confirmation and availability biases. The availability bias is notably interesting. This type of bias is defined by the fact that interpreters focus on models that are available in their minds and thus do not consider a larger range of possible options. In agreement with the same authors, we think that introducing geological knowledge before starting the interpretation will unlock these alternative models and therefore reduce this common, yet difficult to manage, bias. Introducing conscious geological bias also has the advantage of providing tangible justification for the interpretation, thus reducing the subjectivity of the latter (Graafland, 2025). In Geneva, five interpreters investigated GEo-01 and produced different results. The same was observed in the Naaldwijk well in the West Netherlands Basin where academics (Boersma et al., 2021; Cecchetti, 2025) and industry

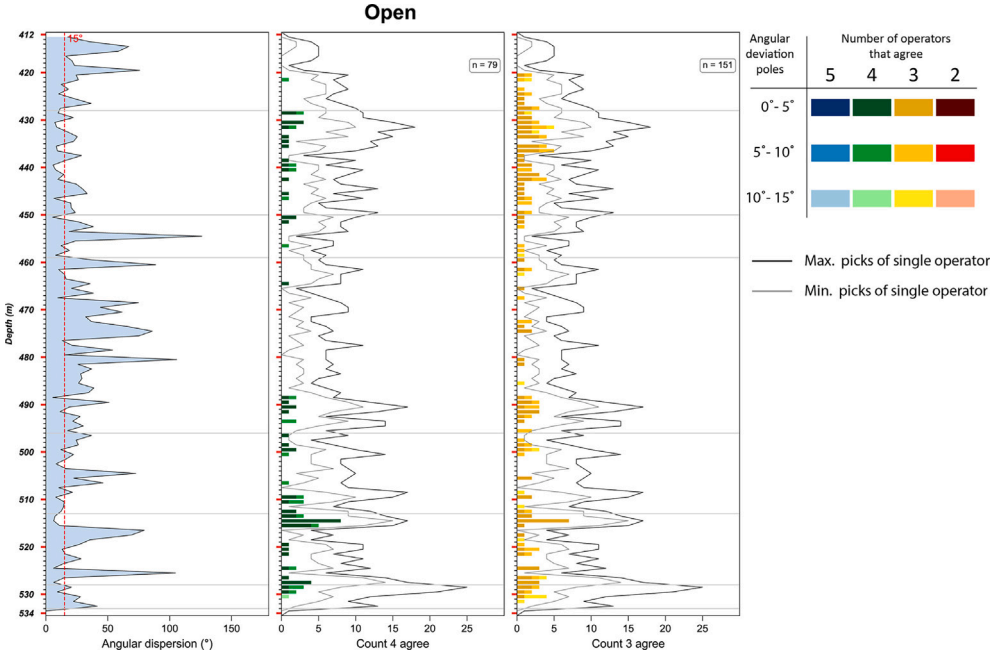


Fig. 12. Angular dispersion of the average orientation of open features (including bedding) identified by four operators, binned per meter (left). The vertical red dashed line marks the 15∘ threshold – a total of 39 m is below the threshold. The bar plots display the number of individual features on which four (middle) and three (right) operators agree, following the methodology explained in Fig. 11. Horizontal lines are the interval boundaries as defined for the frequency of open features (Fig. 9). Intervals of agreement on frequency do not coincide directly with the intervals of orientation agreement.

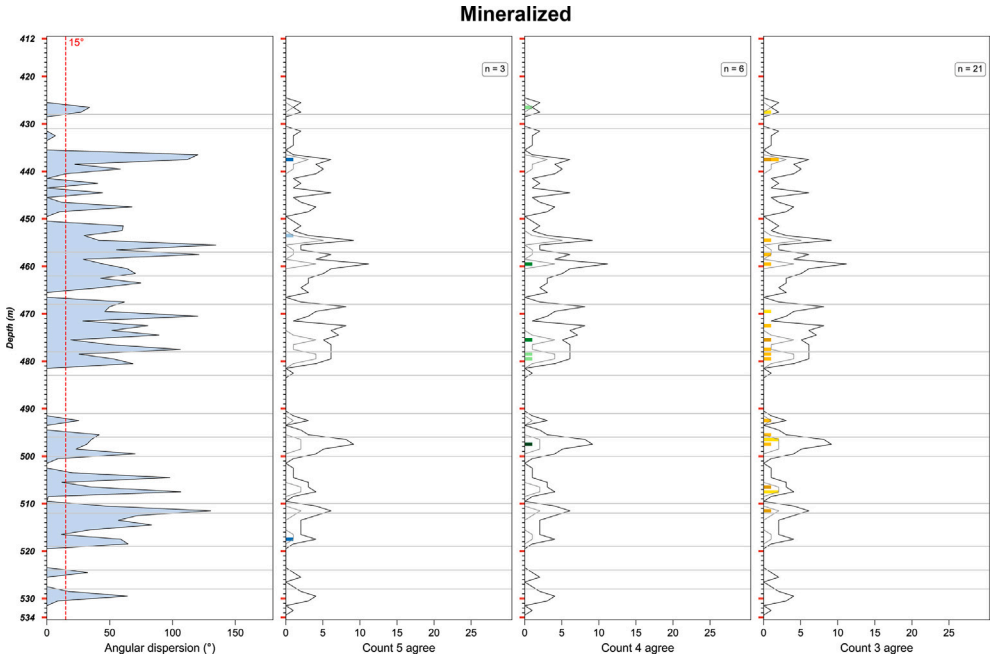


Fig. 13. Angular dispersion of the average orientation of mineralized features identified by five operators, binned per meter (left). The vertical red dashed line marks the 15° threshold - 8 m of the well is below the threshold. Individual features on which five (middle left), four (middle right) and three (right) operators agree on the angular orientation. There are few features on which all five or four out of five operators agree, which hampers a comparison with the intervals defined by the frequency analysis (horizontal lines, Fig. 9). For the legend see Fig. 12.

Table 3
Synthesis of the impact of technical and geological factors on the agreement among different operators on BHI interpretation of GEo-01.

Factor	Feature Picking
Image Complexity	Limited to no impact on frequency and orientation of picking.
Image Quality	Good quality images increases agreement on frequency picking, but may be overridden by the effect of lithology.
Lithology	Largest effect on frequency picking. Bioclastic limestones result in more agreement. Sands, marls, glauconitic sands and hydrocarbon shows result in larger disagreement. Sharp transition in lithology in particular result in disagreement.
Bedding dip	Impact on orientation of features picked, but limited impact on frequency picking. Inclined bedding seems to result in diverging orientations, whereas shallow bedding gives more agreement.

arrived at very different numbers for the amount of natural fractures present in the borehole. Often, disputes like this are decided based on the level of 'expertise' of the interpreter, even though several studies have shown that this is not a relevant factor with respect to subject bias (Bond et al., 2015; Andrews et al., 2019). Instead, we propose that the geological context should decide what is the best interpretation. The lack of support from geological hypotheses is a large gap leaving possible discussions on the level of the experience and expertise of the interpreter, which most of the time remains irrelevant in uncertainty management in fracture interpretation (Andrews et al., 2019).

Potentially the best ways to reduce subjective bias will be to automatize discontinuity picking in wellbore data. Since the first recognition of complex patterns in images from Hough (1962), much research has used this technique to automatically detect fractures in boreholes (e.g., Wang et al., 2007; Assous et al., 2014) and in the field (Prabhakaran et al., 2019). However, these methods suffer from limitations such as computational power involved, lack of flexibility to adjust interpretation and still needing a quality control by an interpreter (Weismüller et al., 2020). Molossi et al. (2025) proposed a deep learning approach based on a convolutional neural network to automatically pick fractures in low resolution logging-while-drilling images. The approach is distinct from the previous ones because it uses synthetic training dataset instead of relying on uncertain interpretations of real images. Remarkably, the method also intends to allow interaction between the algorithm and scientists to introduce flexibility in the interpretation. In this virtuous circle, the algorithm learns from humans and thus sharpens the interpretations. This methodology could be an elegant way to implement the recommendation of (Andrews et al., 2019) to approach fracture picking as a group problem where different skill sets could enhance the validity of the interpretation. The machine learning approach has been tested on BHI data from the West Netherlands Basin and returned promising results for sandstone formations. Even so, a conscious geological bias with respect to the results is still needed to properly understand how the fracture network behaves on a larger scale than just the borehole.

7. Conclusions

This proof-of-concept study constrained factors influencing objective and subjective bias in borehole image interpretation. We used a unique dataset of five interpretations of the same borehole images of the GEo-01 well in the Geneva Basin, Switzerland. Overall, the frequency and orientation analyses of GEo-01 show that:

- Lithology appears to have the largest effect on consistent frequency interpretation. Complexity plays a nuanced role and affects mainly picking counts which modulates disagreement between interpreters. Image quality has an inconsistent impact on frequency agreement between interpreters.
- Bioclastic limestones are generally favorable for agreement between interpreters and provide simpler and better images than other intervals. However, these intervals are less favorable to interpret mineralized features due to poor contrast.
- Marl and sand lithologies combined with the presence of glauconite and hydrocarbon shows create divergence of interpretations

and are generally associated with an increase of image complexity (more features present).
- Highly fractured intervals and sharp transitions between lithologies amplify disagreement, on top of the lithology signal and image quality/complexity effects.
- The agreement among interpreters on fracture orientation is 12% of the total picked open features, which challenges the definition of fracture sets. For mineralized features, the agreement is even lower (4%).
- Intervals with more agreement on orientation do not correspond to interval with more frequency agreement.
- Intervals with low dip angle of bedding surfaces (<35°) appear to result in higher agreements on the fracture orientation.

These findings show that the interpretation of the BHI of GEo-01 is affected by subjective bias. To mitigate this bias, we propose geologically informed guidelines to improve future interpretations of new borehole data in the Geneva Basin. Besides the local aspect, we think that these guidelines can be implemented in any project that involves borehole image interpretations, in order to mitigate the impact of interpretation bias on the characterization of fractures in the subsurface.

CRediT authorship contribution statement

Jasper Hupkes: Writing – original draft, Visualization, Methodology, Investigation, Conceptualization. **Pierre-Olivier Bruna:** Writing – review & editing, Writing – original draft, Supervision, Methodology, Investigation, Conceptualization. **Guillaume Rongier:** Writing – review & editing, Visualization, Methodology. **Giovanni Bertotti:** Writing – review & editing, Supervision, Conceptualization. **Jerôme Caudroit:** Resources. **Andrea Moscariello:** Resources.

Declaration of competing interest

The authors declare that they have no known competing financial interests or personal relationships that could have appeared to influence the work reported in this paper.

Appendix A. Supplementary data

Supplementary data for this article can be found online at doi:10.1016/j.geoen.2026.214793.

Data availability

The BHI data is confidential. All other data used in this paper are available on request, including the code used for analysis.

References

Al-Fahmi, M., Hermawan Manuaba, I., Wang, W., Mat Yaacob, M., 2023. Reservoir fracture detection by LWD and wireline electrical imagers. In: Fifth EAGE Borehole Geology Workshop. European Association of Geoscientists & Engineers, Al Khobar, Al Khobar, Saudi Arabia, pp. 1–8, https://doi.org/10.3997/2214-4609.2023631005

Ameen, M.S., Cosgrove, J.W., 2000. Forced Folds and Fractures. Number 169 in Geological Society Special Edition, The Geological Society, London, https://doi.org/10.1144/gsl.sp.1999.169

Andrews, B.J., Roberts, J.J., Shipton, Z.K., Bigi, S., Tartarello, M.C., Johnson, G., 2019. How do we see fractures? Quantifying subjective bias in fracture data collection. Solid Earth 10, 487–516. https://doi.org/10.5194/se-10-487-2019

Andrews, B.J., Mildon, Z.K., Jackson, C.A., Bond, C.E., 2024. Quantifying fault interpretation uncertainties and their impact on fault seal and seismic hazard analysis. J. Struct. Geol. 184, 105158. https://doi.org/10.1016/j.jsg.2024.105158

Assous, S., Elkington, P., Clark, S., Whetton, J., 2014. Automated detection of planar geologic features in borehole images. Geophysics 79, D11–D19. https://doi.org/10.1190/geo2013-0189.1

Barreiros Jorge, S., 2022. Fracture characterisation in carbonate reservoirs for geothermal production (Master's thesis). TU Delft, Delft.

Bellahsen, N., Mouthereau, F., Boutoux, A., Bellanger, M., Lacombe, O., Jolivet, L., Rolland, Y., 2014. Collision kinematics in the Western external Alps: kinematics of the Alpine collision. Tectonics 33, 1055–1088. https://doi.org/10.1002/2013TC003453

Boersma, Q.D., Bruna, P.O., De Hoop, S., Vinci, F., Moradi Tehrani, A., Bertotti, G., 2021. The impact of natural fractures on heat extraction from tight triassic sandstones in the West Netherlands Basin: a case study combining well, seismic and numerical data. Neth. J. Geosci. 100, e6. https://doi.org/10.1017/njg.2020.21

Bond, C., Gibbs, A., Shipton, Z., Jones, S., 2007. What do you think this is? "Conceptual uncertainty" in geoscience interpretation. GSA Today 17, 4–10. https://doi.org/10.1130/GSAT01711A.1

Bond, C.E., Johnson, G., Ellis, J.F., 2015. Structural model creation: the impact of data type and creative space on geological reasoning and interpretation. Geol. Soc. Lond. Spec. Publ. 421, 83–97. https://doi.org/10.1144/SP421.4

Bourke, L.T., 1992. Sedimentological borehole image analysis in clastic rocks: a systematic approach to interpretation. Geol. Soc. Lond. Spec. Publ. 65, 31–42. https://doi.org/10.1144/GSL.SP.1992.065.01.04

Bourke, L., Prosser, D., Barrett, P., Buchan, C., 2014. Opportunities lost: the value of borehole image logs may be compromised by inadequate quality control. In: EAGE Borehole Geology Workshop, Dubai, United Arab Emirates, https://doi.org/10.3997/2214-4609.20142313

Brentini, M., 2018. Impact d'une donnée géologique hétérogène dans la gestion des géo-ressources: analyse Intégrée Et Valorisation de La Stratigraphie à Travers Le Bassin Genevois (Suisse, France) (Ph.D. thesis). Université de Genève. https://doi.org/10.13097/ARCHIVE-OUVERTE/UNIGE:103409

Caine, J.S., Evans, J.P., Forster, C.B., 1996. Fault zone architecture and permeability structure. Geology 24, 1025–1028. https://doi.org/10.1130/0091-7613(1996)024<1025:FZAAPS>2.3.CO;2

Cecchetti, E., 2025. An Integrated Geological Characterisation of the Lower Triassic Main Buntsandstein Subgroup for Geothermal Applications in the Southern Netherlands (Ph.D. thesis). Delft University of Technology. https://doi.org/10.4233/UUID:C0D6907C-D894-4040-953A-A3B68D5C3F3B

Chatterjee, S., Mukherjee, S., 2023. Review on drilling-induced fractures in drill cores. Mar. Pet. Geol. 151, 106089. https://doi.org/10.1016/j.marpetgeo.2022.106089

Chelle-Michou, C., Do Couto, D., Moscariello, A., Renard, P., Rusillon, E., 2017. Geothermal state of the deep Western Alpine Molasse Basin, France-Switzerland. Geothermics 67, 48–65. https://doi.org/10.1016/j.geothermics.2017.01.004

Choi, J.H., Edwards, P., Ko, K., Kim, Y.S., 2016. Definition and classification of fault damage zones: a review and a new methodological approach. Earth-Sci. Rev. 152, 70–87. https://doi.org/10.1016/j.earscirev.2015.11.006

Clerc, N., Moscariello, A., 2020. A revised structural framework for the Geneva basin and the neighbouring France region as revealed from 2D seismic data: implications for geothermal exploration. Swiss Bull. angew. Geol. 25, 109–131. https://doi.org/10.5169/seals-977312

Do Couto, D., Garel, S., Moscariello, A., Bou Daher, S., Littke, R., Weniger, P., 2021. Origins of hydrocarbons in the Geneva Basin: insights from oil, gas and source rock organic geochemistry. Swiss J. Geosci. 114, 11. https://doi.org/10.1186/s00015-021-00388-4

Doesburg, M., 2023. Uncertainty Reduction in Image Log Fracture Interpretation, and Its Implications to the Geological History of the Geneva Basin, Switzerland (Master's thesis). TU Delft, Delft.

Eruteya, O.E., Crinière, A., Moscariello, A., 2024. Seismic expression of paleokarst morphologies and associated siderolithic infill in the Geneva Basin, Switzerland: implications for geothermal exploration. Geothermics 117, 102868. https://doi.org/10.1016/j.geothermics.2023.102868

Fernández-Ibáñez, F., DeGraff, J., Ibrayev, F., 2018. Integrating borehole image logs with core: a method to enhance subsurface fracture characterization. AAPG Bull. 102, 1067–1090. https://doi.org/10.1306/0726171609317002

Graafland, T.W., 2025. The Impact of Prior Geological Knowledge on the Interpretation of Fracture Characterization (Master's thesis). TU Delft, Delft.

Guglielmetti, L., Heidinger, M., Eichinger, F., Moscariello, A., 2022. Hydrochemical characterization of groundwaters' fluid flow through the upper mesozoic carbonate geothermal reservoirs in the Geneva basin: an evolution more than 15, 000 years long. Energies 15, 3497. https://doi.org/10.3390/en15103497

Hough, P.V., 1962. Method and means for recognizing complex patterns. US Patent 3069654. https://www.osti.gov/biblio/4746348.

Howell, J.A., Martinius, A.W., Good, T.R., 2014. The application of outcrop analogues in geological modelling: a review, present status and future outlook. Geol. Soc. Lond. Spec. Publ. 387, 1–25. https://doi.org/10.1144/SP387.12

Hupkes, J., Bruna, P.O., Bertotti, G., Doesburg, M., Moscariello, A., 2026. A fracture rarely comes alone: associations of fractures and stylolites in analogue outcrops improve borehole image interpretations of fractured carbonate geothermal reservoirs. Solid Earth 17, 113–134. https://doi.org/10.5194/se-17-113-2026

Kalifi, A., Leloup, P.H., Sorrel, P., Galy, A., Demory, F., Spina, V., Huet, B., Quillévéré, F., Ricciardi, F., Michoux, D., Lecacheur, K., Grime, R., Pittet, B., Rubino, J.L., 2021. Chronology of thrust propagation from an updated tectono-sedimentary framework of the miocene molasse (Western Alps). Solid Earth 12, 2735–2771. https://doi.org/10.5194/se-12-2735-2021

Khoshbakht, F., Azizzadeh, M., Memarian, H., Nourozi, G., Moallemi, S., 2012. Comparison of electrical image log with core in a fractured carbonate reservoir. J. Pet. Sci. Eng. 86-87, 289–296. https://doi.org/10.1016/j.petrol.2012.03.007

Koumrouyan, M., 2019. Geomechanical Characterisation of Geothermal Exploration Borehole: Implication for the GEo0-01 Well, in Geneva (Master's thesis). Université de Neuchâtel, Neuchâtel.

Lai, J., Wang, G., Wang, S., Cao, J., Li, M., Pang, X., Han, C., Fan, X., Yang, L., He, Z., Qin, Z., 2018. A review on the applications of image logs in structural analysis and sedimentary characterization. Mar. Pet. Geol. 95, 139–166. https://doi.org/10.1016/j.marpetgeo.2018.04.020

Laubach, S.E., Baumgardner, R.W., Monson, E.R., Hunt, E., Meador, K.J., 1988. Fracture detection in low-permeability reservoir sandstone: a comparison of BHTV and FMS logs to core. In: SPE Annual Technical Conference and Exhibition. SPE, Houston, Texas. pp. SPE–18119–MS. https://doi.org/10.2118/18119-MS

Li, X., Li, C., Yao, H., Gong, W., 2024. Probabilistic analysis of seepage and temperature fields in geothermal extraction process based on discrete fracture network (DFN)

model. Appl. Therm. Eng. 254, 123688. https://doi.org/10.1016/j.applthermaleng.2024.123688
Lo, H.Y., 2019. Discrete Fracture Network Modelling in the Geneva Basin (Lower Cretaceous Carbonates): Implication for Geothermal Exploration (Master's thesis). Université de Genève, Geneva.
Lorenz, J.C., Cooper, S.P., 2020. Applied Concepts in Fractured Reservoirs. Wiley Blackwell, Chichester.
Lucca, A., Mittempergher, S., Succo, A., Bistacchi, A., Meda, M., Storti, F., 2023. Deformation sequence and paleofluids in carbonate buckle folds under transpression (pag anticline, external dinarides, Croatia). Tectonics 42, e2023TC007781. https://doi.org/10.1029/2023TC007781
Marro, A., Hauvette, L., Borderie, S., Mosar, J., 2023. Tectonics of the Western internal Jura fold-and-thrust belt: 2D kinematic forward modelling. Swiss J. Geosci. 116, 10. https://doi.org/10.1186/s00015-023-00435-2
Mayolle, S., Soliva, R., Dominguez, S., Wibberley, C., 2023. Normal fault damage zone growth in map view from analogue models. J. Struct. Geol. 176, 104975. https://doi.org/10.1016/j.jsg.2023.104975
Micarelli, L., Benedicto, A., Wibberley, C., 2006. Structural evolution and permeability of normal fault zones in highly porous carbonate rocks. J. Struct. Geol. 28, 1214–1227. https://doi.org/10.1016/j.jsg.2006.03.036
Molossi, A., Cecchetti, E., Bruna, P.O., Pipan, M., 2025. Deep learning-assisted borehole image analysis for enhanced geothermal reservoir evaluation: a case study in the west Netherlands basin. Geoenergy 3, geoenergy2025–009. https://doi.org/10.1144/geoenergy2025-009
Moscariello, A., 2019. Exploring for geo-energy resources in the Geneva Basin (Western Switzerland): opportunities and challenges. Swiss Bull. fuer angew. Geol. 24, 105–124.
Ortega, O.J., Marrett, R.A., Laubach, S.E., 2006. A scale-independent approach to fracture intensity and average spacing measurement. AAPG Bull. 90, 193–208. https://doi.org/10.1306/08250505059
Peacock, D., Mann, A., 2005. Evaluation of the controls on fracturing in reservoir rocks. J. Pet. Geol. 28, 385–396. https://doi.org/10.1111/j.1747-5457.2005.tb00089.x
Playton, T., Earnest, E., Fernández-Ibáñez, F., Bibolova, A., Tolessin, D., Tussupbayev, I., Toleubay, B., 2025. Fracture characterization from core and image log integration at Tengiz and Korolev fields, Kazakhstan. AAPG Bull. 109, 807–843. https://doi.org/10.1306/04292523089
Prabhakaran, R., Bruna, P.O., Bertotti, G., Smeulders, D., 2019. An automated fracture trace detection technique using the complex shearlet transform. Solid Earth 10, 2137–2166. https://doi.org/10.5194/se-10-2137-2019
Ringrose, P.S., Martinius, A.W., Alvestad, J., 2008. Multiscale geological reservoir modelling in practice. Geol. Soc. Lond. Spec. Publ. 309, 123–134. https://doi.org/10.1144/SP309.9
Rusillon, E., 2017. Characterisation and Rock Typing of Deep Geothermal Reservoirs in the Greater Geneva Basin (Switzerland & France) (Ph.D. thesis). Université de Genève. https://doi.org/10.13097/ARCHIVE-OUVERTE/UNIGE:105286
Schegg, R., Leu, W., 1998. Analysis of erosion events and palaeogeothermal gradients in the North Alpine Foreland Basin of Switzerland. Geol. Soc. Lond. Spec. Publ. 141, 137–155. https://doi.org/10.1144/GSL.SP.1998.141.01.09
Scotese, C., Schettino, A., 2017. Late permian-early jurassic paleogeography of Western Tethys and the World. In: Permo-Triassic Salt Provinces of Europe, North Africa and the Atlantic Margins. Elsevier, pp. 57–95. https://doi.org/10.1016/B978-0-12-809417-4.00004-5
Smith, R.Y., Bruna, P.O., Nasri, A., Bertotti, G., 2024. Fracture distribution along open folds in southern Tunisia: implications for naturally fractured reservoirs. Pet. Geosci. 30, petgeo2023–039. https://doi.org/10.1144/petgeo2023-039
Sommaruga, A., 1999. Décollement tectonics in the Jura forelandfold-and-thrust belt. Mar. Pet. Geol. 16, 111–134. https://doi.org/10.1016/S0264-8172(98)00068-3
Strasser, A., Charollais, J., Conrad, M.A., Clavel, B., Pictet, A., Mastrangelo, B., 2016. The cretaceous of the Swiss Jura Mountains: an improved lithostratigraphic scheme. Swiss J. Geosci. 109, 201–220. https://doi.org/10.1007/s00015-016-0215-6
Torabi, A., Rudnicki, J., Alaei, B., Buscarnera, G., 2023. Envisioning faults beyond the framework of fracture mechanics. Earth-Sci. Rev. 238, 104358. https://doi.org/10.1016/j.earscirev.2023.104358
Wang, W.H., Thagafy, M.M., 2017. Applications of high-resolution LWD resistivity image logs for Carbonate Reservoir characterization. In: SPE Kingdom of Saudi Arabia Annual Technical Symposium and Exhibition. SPE, Dammam, Saudi Arabia. p. D043S041R002. https://doi.org/10.2118/188115-MS
Wang, W., Liao, H., Huang, Y., 2007. Rock fracture tracing based on image processing and SVM. In: Third International Conference on Natural Computation (ICNC 2007). IEEE, Haikou, China, pp. 632–635, https://doi.org/10.1109/ICNC.2007.643
Watkins, H., Butler, R.W., Bond, C.E., Healy, D., 2015. Influence of structural position on fracture networks in the Torridon Group, achnashellach fold and thrust belt, NW Scotland. J. Struct. Geol. 74, 64–80. https://doi.org/10.1016/j.jsg.2015.03.001
Wedge, D., Holden, E.J., Dentith, M., Spadaccini, N., 2015. Automated structure detection and analysis in televiewer images. ASEG Ext. Abstr. 2015, 1–4. https://doi.org/10.1071/ASEG2015ab152
Weismüller, C., Prabhakaran, R., Passchier, M., Urai, J.L., Bertotti, G., Reicherter, K., 2020. Mapping the fracture network in the lilstock pavement, Bristol Channel, UK: manual versus automatic. Solid Earth 11, 1773–1802. https://doi.org/10.5194/se-11-1773-2020
Wellmann, F., Caumon, G., 2018. 3-D structural geological models: concepts, methods, and uncertainties. In: Advances in Geophysics, vol. 59. Elsevier, pp. 1–121. https://doi.org/10.1016/bs.agph.2018.09.001
Williams, J.H., Johnson, C.D., 2004. Acoustic and optical borehole-wall imaging for fractured-rock aquifer studies. J. Appl. Geophys. 55, 151–159. https://doi.org/10.1016/j.jappgeo.2003.06.009
Wood, D.A., 2024. Expanding role of borehole image logs in reservoir fracture and heterogeneity characterization: a review. Adv. Geo-Energy Res. 12, 194–204. https://doi.org/10.46690/ager.2024.06.04